Application of kaolin-Fe$_3$O$_4$ nano-composite for the removal of azo dye from aqueous solutions

Azita Mohagheghian[a], Melina Pourmohseni[a], Robabeh Vahidi-Kolur[a], Jae-Kyu Yang[b], Mehdi Shirzad-Siboni[a,c,d,]*

[a]*Department of Environmental Health Engineering, School of Health, Guilan University of Medical Sciences, Rasht, Iran,
Tel. +98 9111309440; email: mohagheghian@yahoo.com (A. Mohagheghian), Tel. +98 9117390924;
email: melina.mohseni80@gmail.com (M.Pourmohseni), Tel. +98 9111850017; email: rvahidikolur@yahoo.com (R. Vahidi-Kolur)*
[b]*Ingenium College of Liberal Arts, Kwangwoon University, Seoul, Korea, Tel. +82 2 940 5769; email: jkyang@kw.ac.kr*
[c]*Research Center of Health and Environment, Guilan University of Medical Sciences, Rasht, Iran*
[d]*Department of Environmental Health Engineering, School of Public Health, Iran University of Medical Sciences, Tehran, Iran,
Tel. +98 9112346428; Fax: +98 1333849413; email: mshirzadsiboni@yahoo.com*

abstract

Kaolin-Fe$_3$O$_4$ nanoparticles synthesized by co-precipitation and hydrothermal methods was used to remove Acid Red 14 (AR14) from aqueous solutions at various pH, dye concentrations, adsorbent dosages, temperatures and ionic strength. Efficient coating of Fe$_3$O$_4$ nanoparticles onto Kaolin was identified by FT-IR, XRD, SEM, EDX and VSM analysis. Removal efficiency of AR14 by Kaolin-Fe$_3$O$_4$ nanoparticles was greater than that by Kaolin-alone and Fe$_3$O$_4$-alone. Maximum adsorption was obtained at pH 3. The removal efficiency was increased with increasing adsorbent dosage, but was decreased with increasing initial AR14 concentration and temperature. Removal efficiency of AR14 decreased in the presence of four selected anions. Adsorption kinetic was well described by pseudo-second order model. Adsorption isotherm was well described by the Langmuir equation. Maximum adsorption capacity was 94.34 mg/g. Thermodynamic studies indicated adsorption of AR14 onto kaolin-Fe$_3$O$_4$ nanoparticles through an exothermic process. Adsorption activity of AR14 by kaolin-Fe$_3$O$_4$ nanoparticles was maintained even after six successive cycles. Kaolin-Fe$_3$O$_4$ can be used for the treatment of aqueous solutions containing dyes as an efficient adsorbent and can be easily separated from solution by magnet after reaction.

Keywords: Nanoparticles; Kaolin-Fe$_3$O$_4$; Kinetic and Isotherm models; Thermodynamics, Adsorption; Acid Red 14

1. Introduction

Organic dyes have been applied in several industries such as textile, paper, cosmetic, leather, plastics, food, printing and pharmaceuticals [1,2]. Contamination of dyes in water can cause less penetration of sunlight, gas solubility, and photosynthesis and is regarded as serious threats to the aquatic systems [3,4]. Acid Red 14 (disodium 4-hydroxy-2-[(*E*)-(4-sulfonato-1-naphthyl)diazenyl]naphthalene-1-sulfonate) is a synthetic red dye having -N=N- functional group which is resistant to biodegradation and has very toxic, mutagenic and carcinogenic properties [5]. Therefore, water systems contaminated with organic dyes should be treated with suitable physicochemical and/or biological treatment processes [6–8]. Biological treatment has some limitations in the treatment of dyes due to stability and complexity of the aromatic structure [9,10]. Several physicochemical processes such as filtration [11], chemical precipitation [12], electro-deposition [13], electro-coagulation [14],

---

* Corresponding author.

advanced oxidation [5,6,15] and ion exchange [16] have been applied. However, some of these processes have several disadvantages such as formation of hazardous byproducts, high initial installation cost, generation of chemical wastes, and high energy requirement [5,13, 16–18]. Among several physicochemical processes, adsorption technique has much attention because it is simple, efficient, and requires low operating cost. Generally, activated carbon has been widely used as an efficient adsorbent [19,20]. However, it has limitation in large-scale application due to the relatively high preparation cost [19,20]. To compensate this limitation, sawdust [21], agricultural residues [22], activated red mud [23] and fly ash [24], dolomite [25], oyster shell [26], activated sludge [27], furnace slag [28], chitosan [29], and scallop shell [30] have been applied to treat wastewater as low-cost adsorbents. When adsorption capacity of these adsorbents has been exhausted, they should be separated from the aquatic system using filtration method and regenerated. However, filtration is a tedious process causing filter blockages [4,31]. Kaolin, a kind of clay materials, has an aluminosilicate composition with crystalline structure, which consists of stacked pairs of tetrahedral SiO_2 and octahedral Al_2O_3 sheets [32,33]. It has high removal potential for heavy metal ions through adsorption and can be used as a supporting material for the catalytic processes due to its large surface area and pore volume [32,33]. As kaoline has multifunctional properties, it was used for the synthesis of new materials [20]. Recently, magnetic separation has much attention as a promising environmental technique since it produces no contaminants and has the ability to treat large amount of wastewater within a short span of time [34–36]. Fe_3O_4 is a traditional magnetic material having superparamagnetic property [34–36]. It can be recovered very quickly by external magnetic field and reused without losing its active sites [34–36]. Hence, the kaolin particles combined with Fe_3O_4 can be used as an alternative to the traditional adsorbents for large scale wastewater treatment processes.

A number of studies have been reported for the removal of dyes with kaolin alone, such as removal of the brilliant green dye [20], congo red [37], methylene blue (MB) [7], crystal violet [32], basic yellow 28 (BY28) [33] and malachite green (MG) [33]. Also there are many reports about removal of dyes with magnetite alone and magnetite nanocomposites such as Fe_3O_4-activated carbon nanocomposite [35], $Fe_3O_4@C$ nanoparticles [36], chitosan/kaolin/γ-Fe_2O_3 composites [38], cellulose/Fe_3O_4/activated carbon composite [38], Fe_3O_4/ZrO_2/Chitosan composite [39], $Fe_3O_4@$graphene nanocomposite [40]. However, limited information is available for the removal efficiency and removal kinetics of dyes using natural adsorbent magnetized with Fe_3O_4 in the presence of ionic compounds having different functional groups with aim of easy separation.

In this study, kaolin-Fe_3O_4 nanoparticles were used for the adsorption of acid red 14 (AR14) from aqueous solutions. The effects of pH, adsorbent dosage, initial AR14 concentration, ionic strength (sodium carbonate, sodium bicarbonate, sodium sulfate and sodium chloride) and temperature on the removal efficiency were studied. Adsorption kinetic, isotherm and thermodynamic studies were undertaken to comprehend the adsorption mechanism and maximum adsorption capacity of kaolin-Fe_3O_4 nanoparticles.

2. Materials and methods

2.1. Chemicals

Iron(III) chloride ($FeCl_3.6H_2O$), Iron(II) chloride ($FeCl_2.4H_2O$), sodium hydroxide, hydrogen peroxide, sodium chloride, sodium sulphate, sodium hydrogen carbonate, sodium carbonate, and hydrochloric acid, which were of analytical grade, were purchased from Merck, Germany and used without any purification. Kaolin powder was obtained from Ideal Trades Men Company in Qazvin city from Iran. It was washed with deionized water, dried at 103°C for 3 h in an oven and then sieved in the size range of 50 meshes ASTM. The main composition was SiO_2 (46.13%), Al_2O_3 (26.98%) and K_2O (2%) according to above company. Acid Red 14 was purchased from Alvan Sabet Co., Iran. The chemical structure of AR14 has been presented in Table 1 [41]. The initial pH of solution was adjusted by the addition of 0.1 M NaOH or HCl, and measured by pH meter (Metron, Switzerland). The experiments were carried out at room temperature (25 ± 2°C). AR14 stock solution (1,000 mg/L) was prepared in distilled water and kept in dark.
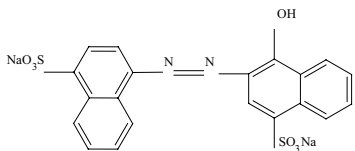
2.2. Magnetization of the kaolin-Fe_3O_4 nanoparticles

Kaolin-Fe_3O_4 nanoparticles particles were prepared via the co-precipitation and hydrothermal methods in alkaline solution [42]. The appropriate amount of $FeCl_3.6H_2O$ and $FeCl_2.4H_2O$ were dissolved in 200 mL deionized water. Kaolin was added to the suspension at 1:1 volume ratio. NH_4OH 25% (25 mL) was added drop-wise to the precursor solution to obtain an alkaline medium (pH = 8) producing a black and gelatinous precipitate of kaolin-Fe_3O_4 nanoparticles under nitrogen gas. It was heated at 80°C for 2 h with continuous stirring. The desired kaolin-Fe_3O_4 nanoparticles was collected by a permanent magnet and then washed with deionized water and ethanol for 5 times. Then it was dried at 80°C in vacuum for 5 h.

2.3. Characterization instruments

For characterization of the functional groups on the surface of the samples, Fourier transform infrared spectroscopy (FT-IR) spectra were recorded using a Perkin-Elmer (Germany) spectrometer under dry air at room

Table 1
The structure and characteristics of C.I. Acid Red 14

Color index name	C.I. Acid Red 14
Chemical structure	
Chemical class	Anionic, Azo
Molecular formula	$C_{20}H_{12}Na_2N_2O_7S_2$
Color index number	14720
λ_{max} (nm)	515
M_w (g/mol)	502.43

temperature by the KBr pellets method. The spectra were collected over the range from 400 to 4,000 cm⁻¹. The X-ray diffraction (XRD) studies were performed with a Philips XRD instrument (Siemens D-5000, Germany) using Cu Kα radiation (λ = 1.5406 Å) at wide-angle range (2θ value 4–70°) at 40 kV of accelerating voltage and at 30 mA of emission current. The surface morphology of kaolin, Fe_3O_4 and kaolin-Fe_3O_4 nanoparticles were obtained by a field emission scanning electron microscopy (Mira3, Tescan, Czech Republic). SEM images were further supported by energy dispersive X-ray (EDX) to provide direct evidence for the purity, existence and distribution of specific elements in a solid sample. The magnetic property of kaolin-Fe_3O_4 nanoparticles was characterized by Vibrating Sample Magnetometer (VSM, MDKFD, Iran). The point of zero charge (pH$_{pzc}$) was determined to investigate the surface charge properties of the adsorbents. The pH$_{PZC}$ of kaolin-Fe_3O_4 nanoparticles was determined adopting the method previously used [30,43].

2.4. Adsorption experiments

All adsorption experiments were carried out in 1,000 mL Erlenmeyer flask containing both AR14 and kaolin-Fe_3O_4 nanoparticles. The mixtures were continuously stirred (150 rpm) at room temperature in different time intervals (2–120 min). Then adsorbent was separated from the mixture solution by permanent magnet. The concentration of the AR14 in each sample was measured using a spectrophotometer (UV/Vis Spectrophotometer, Hach-DR 5000, USA) at λ_{max} = 515 nm by a calibration curve [44]. In order to study effects of various parameters, experiments were conducted at different amounts of adsorbent (0.1 to 0.4 g/L), initial dye concentrations (10 to 120 mg/L), initial pH (2 to 11) and temperature (298 to 323 K). The removed amount of dye by kaolin-Fe_3O_4 nanoparticles and removal efficiency were calculated by Eqs. (1) and (2), respectively [7,32].

$$q = \frac{(C_o - C_e)V}{M} \times 100 \tag{1}$$

$$\text{Removal efficiency (\%)} = \frac{(C_i - C_o)}{C_i} \times 100 \tag{2}$$

where, q is the adsorption capacity (mg/g). C_i, C_0 and C_e are the initial, outlet and equilibrium concentrations of dye (mg/L), respectively. V is the volume of dye solution (L) and M is the total amount of kaolin-Fe_3O_4 nanoparticles (g).

3. Results and discussion

3.1. Adsorbent characterization

3.1.1. FT-IR analysis

FT-IR analysis of kaolin, Fe_3O_4 and kaolin-Fe_3O_4 nanoparticles were performed in the range of 400 to 4,000 cm⁻¹ (Fig. 1). The kaolin showed significant absorption peaks at 469.59, 534.62, 692.97, 794.35, 915.03, 1006.39, 1037.70, 3622.96 and 3699.31 cm⁻¹. Fe_3O_4 nanoparticles showed significant absorption peaks at 447; 580; 860; 1,403; 1,623; 3,378 3,788 and 3,850 cm⁻¹. Kaolin-Fe_3O_4 nanoparticles showed significant absorption peaks at 465; 574; 790; 1,029;
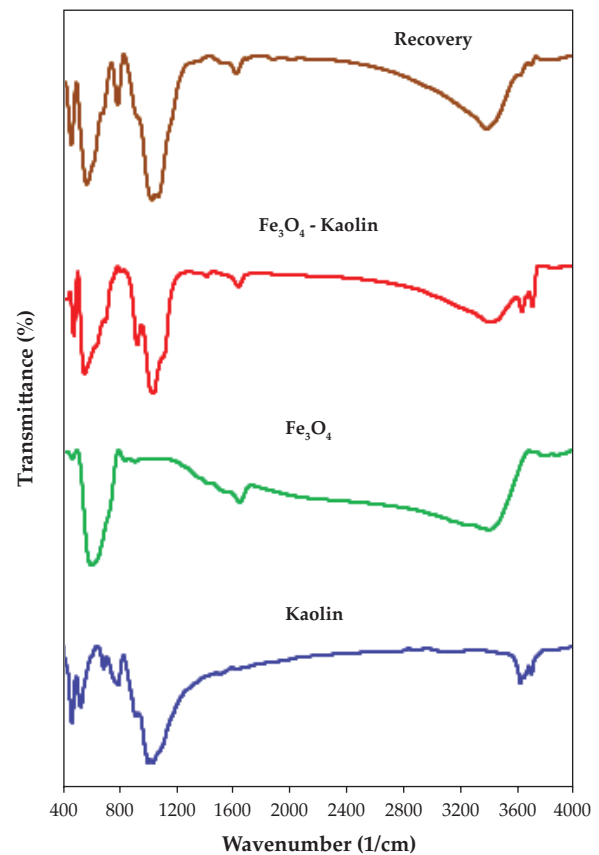

Fig. 1. FT-IR spectra of samples.

1,625; 3,385 and 3,858 cm⁻¹. The two distinct absorption peaks observed at 580 and 447 cm⁻¹ are attributed to the vibrations of Fe^{3+}–O^{2-} and Fe^{2+}–O^{2-}, respectively. Three bands or peaks observed at 3,378, 3,788 and 3,850 cm⁻¹ have been attributed to hydroxyl group. The peak obtained at 1,403 cm⁻¹ may correspond to vibration of H–O–H [35,39]. Moreover, the peak appeared at 3,665 cm⁻¹ for kaolin corresponds to the –OH stretching band of Al–OH and Si–OH. The peak at 1,037 cm⁻¹ corresponds to the Si–O–Si stretching (in-plane) vibration for layered silicates. The FT-IR analysis supported coating of Fe_3O_4 nanoparticles onto kaolin [45].

3.1.2. XRD analysis

The XRD patterns of kaolin, Fe_3O_4 and kaolin-Fe_3O_4 nanoparticles are illustrated in Fig. 2. The patterns exhibit crystalline structure of both kaolin and Fe_3O_4 even after coating of Fe_3O_4 nanoparticles onto kaolin. The main peaks at 2θ values of 18.27, 21.16, 30.11, 30.21, 35.42, 35.53, 37.03, 37.18, 43.12 and 57.09 were correspond to the (011), (002), (112), (200), (121), (103), (022), (202), (004) and (321) planes of orthorhombic Fe_3O_4 (JCPDS card no. 031156). As illustrated in Fig. 2, the peaks related to the Fe_3O_4 nanoparticles are still observed after the coating of Fe_3O_4 nanoparticles onto kaolin. This result indicates growth of the Fe_3O_4 nanoparticles crystal on the kaolin. The average crystalline size of Fe_3O_4 and kaolin-Fe_3O_4 nanoparticles were calculated using the following Debye–Sherrer's equation (Eq. 3):
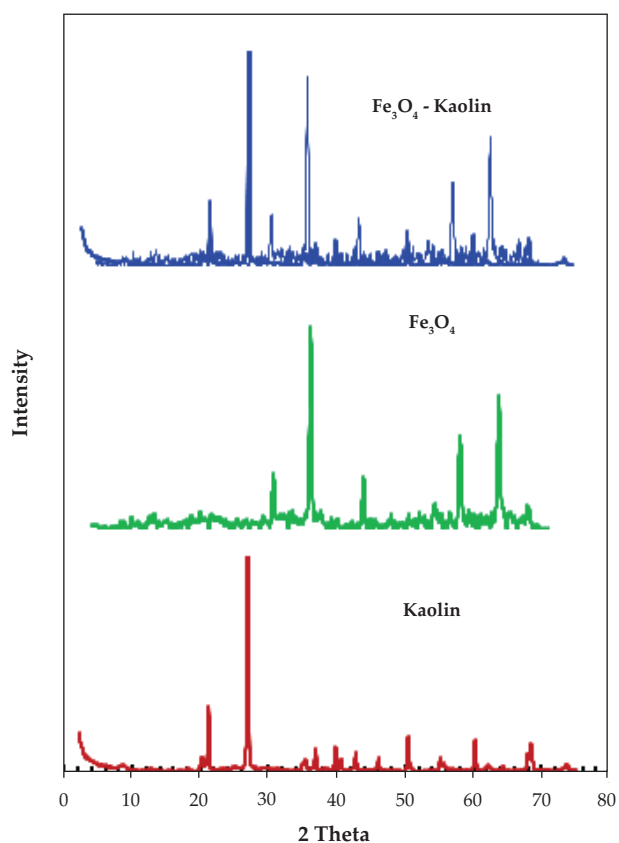
Fig. 2. Typical XRD patterns of samples.

$$D = \frac{0.9\lambda}{\beta \mathrm{Cos}\theta} \qquad (3)$$

where D is the average crystallite size (Å), λ is the wavelength of the X-ray radiation (Cu $K\alpha$ = 1.54178 Å), β is the full width at half maximum intensity of the peak and θ is the diffraction angle. According to the Eq. (3), the mean crystallite size of the Fe_3O_4 and kaolin-Fe_3O_4 nanoparticles were estimated to be 8 and 22 nm, respectively.

3.1.3. SEM, EDX and VSM analysis

SEM images of kaolin, Fe_3O_4 and kaolin-Fe_3O_4 nanoparticles are shown in Figs. 3a, b and c, respectively. Fig. 3c clearly illustrates the distribution of magnetite nanoparticles over the surface of the kaolin. The size of Fe_3O_4 nanoparticles was around 20 nm. EDX microanalysis was used to characterize the elemental composition of the Fe_3O_4 and kaolin-Fe_3O_4 nanoparticles. EDX pattern of the Fe_3O_4 and kaolin-Fe_3O_4 nanoparticles is depicted in Fig. 4. According to the EDX analysis, the major elements were Fe, O, Al, Si and K and Fe, indicating good hybridization between kaolin and Fe_3O_4 nanoparticles. VSM was used to measure property of Fe_3O_4 and kaolin-Fe_3O_4 nanoparticles. VSM magnetization curve of the Fe_3O_4 and kaolin-Fe_3O_4 nanoparticles at room temperature is depicted in Fig. 5. The saturated magnetization value of Fe_3O_4 and kaolin-Fe_3O_4 nanoparticles was 58.97 and 36.83 emu/g, respectively. These results also indicated that
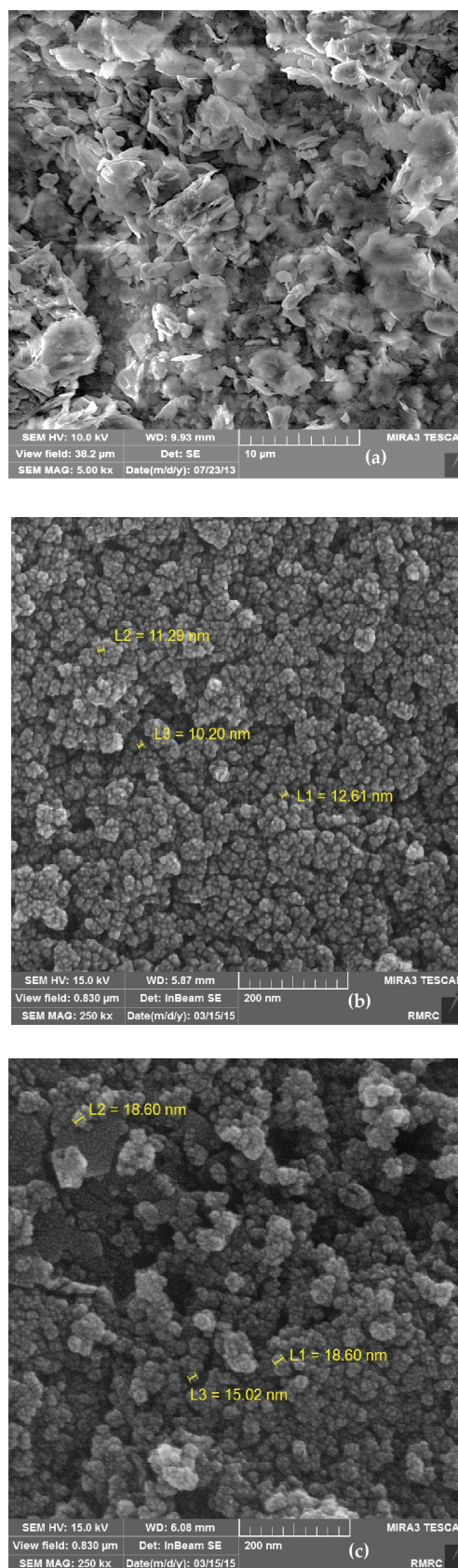

Fig. 3. SEM image of samples (a) Kaolin, (b) Fe_3O_4 nanoparticles, (c) Kaolin coated with Fe_3O_4 nanoparticles.
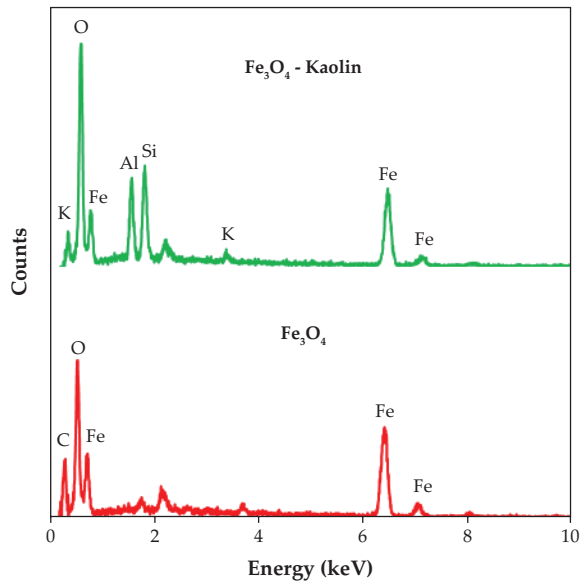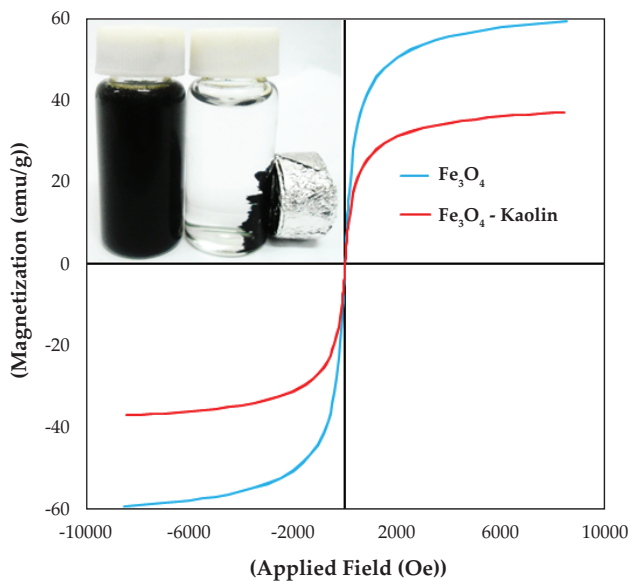
Fig. 4. EDX image of samples.

Fig. 5. VSM image of samples.

the kaolin-Fe_3O_4 nanoparticles showed an excellent magnetic response to a magnetic field. Therefore, it could be separated easily and rapidly due to this high magnetic sensitivity. This value is greater than the magnetization value of $Fe_3O_4@C$ (6.94 emu/g) [36], Fe_3O_4-activated carbon nanocomposite (2.78 emu/g) [35] reported by other researchers.

3.2. Effect of parameters on the removal of AR14 with kaolin-Fe_3O_4 nanoparticles

3.2.1. The effect of solution pH

The effect of pH on the AR14 (30 mg/L) adsorption onto kaolin-Fe_3O_4 nanoparticles (0.24 g/L) was investigated between pH 2 to 11 and the results are depicted in
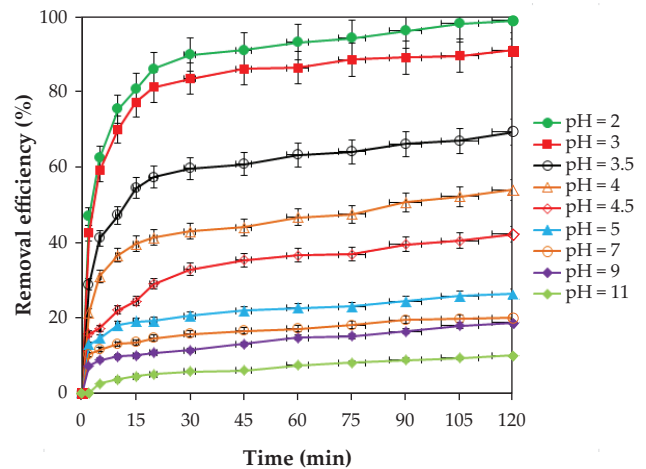

Fig. 6. The effect of pH on the removal of AR14 dye by kaolin coated with Fe_3O_4 nanoparticles in different time interval (initial dye concentration = 30 mg/L, adsorbent dose = 0.24 g/L, 298 K).

Fig. 6. Solution pH is recognized as one of the important parameters that governs the adsorption process. Fig. 6 shows that removal efficiency decreased by increasing the solution pH. Indeed, the removal efficiency decreased from 98.63 to 9.98% by increasing the solution pH from 2 to 11. Generally, surface charge of the adsorbents and speciation of ionic contaminants is variable with variation of solution pH. Maximum removal efficiency of AR14 was observed at pH 2. The variation of dye uptake with respect to the initial solution pH can be explained by the structure of dye molecule as well as pH_{pzc} value of kaolin-Fe_3O_4 nanoparticles. According to the data, the pH_{pzc} of Fe_3O_4 and kaolin-Fe_3O_4 nanoparticles are 6 and 6.66, respectively. The pH_{pzc} for kaolin was reported as 7. On the other hand, the kaolin-Fe_3O_4 nanoparticles acquires a negative surface charge above this pH since the pH_{pzc} of kaolin-Fe_3O_4 nanoparticles is 6.66 [31,35,43]. At a pH lower than pH_{pzc} the surface of kaolin-Fe_3O_4 nanoparticles acquires positive charge and dye molecules also has less negative charge [31,35,43]. The pK_a value of AR14 is known as 6.7 [46]. Considering the pH_{pzc} of Fe_3O_4 and kaolin-Fe_3O_4 nanoparticles and the pK_a value of AR14, maximum adsorption was expected around neutral pH; however, the greatest removal was observed at pH 2. It was difficult to explain this trend in this work. Even though the greatest removal was observed at pH 2, the other experiments were performed at pH 3 because there was only a little difference of removal efficiency between pH 2 and pH 3 as well as requiring much acid for adjusting the solution pH at 2.

3.2.2. The effect of adsorbent dosage and contact time

The influence of adsorbent dosage on the removal efficiency for AR14 was investigated at various amounts of kaolin-Fe_3O_4 nanoparticles in the range of 0.1 to 0.4 g/L at pH3 with variation of reaction time (Fig. 7). Indeed, the removal efficiency increased from 44.05 to 99.31% by increasing the adsorbent dosage from 0.1 to 0.4 g/L over the entire reaction time (2–120 min). This trend can be explained by
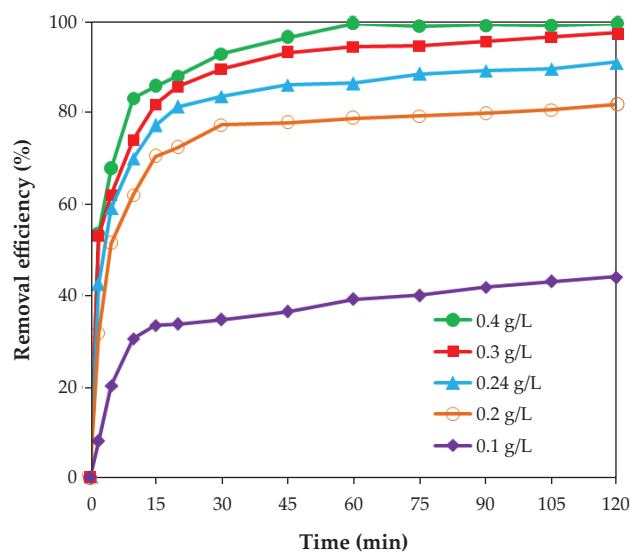
Fig. 7. The effect of adsorbent dose on the removal of AR14 dye by kaolin coated with Fe_3O_4 nanoparticles in different time interval (initial dye concentration = 30 mg/L, pH = 3, 298 K).
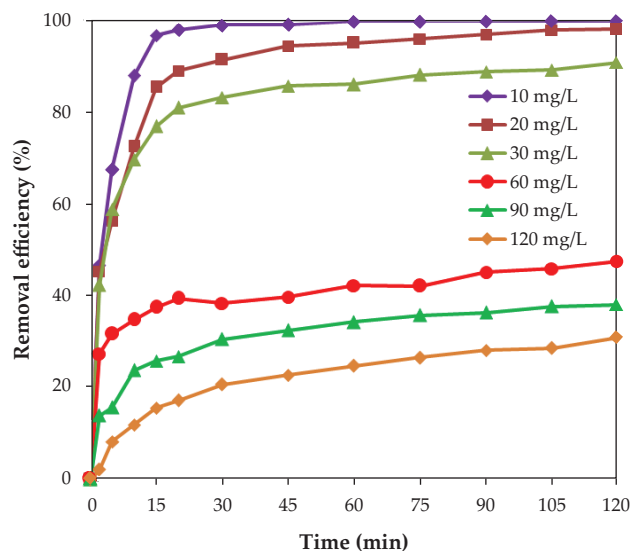

Fig. 8. The effect of initial AR14 dye concentration on the removal of AR14 dye by kaolin coated with Fe_3O_4 nanoparticles in different time interval (pH= 3, adsorbent dose = 0.24 g/L, 298 K).

the increased active sites for the removal of contaminants along with the increase of the adsorbent dosage. As shown in Fig. 7, the removal rate of AR14 at all dosages was rapid in the initial reaction time (before 45 min) and then it was gradually slowed until reactions reach a near equilibrium after 120 min. The rapid adsorption at initial reaction time may be attributed to the abundance of free active sites on the surface of kaolin-Fe_3O_4 nanoparticles and easy availability of them for AR14 molecules [4,34]. As the active sites are occupied by AR14, adsorption rates are decreased due to having little available active sites on the adsorbents [4,34]. Since the removal efficiency of AR14 was not much different between dosage 0.24 g/L and 0.4 g/L (almost 8.47%), further experiments were performed at 0.24 g/L.

3.2.3. The effect of initial AR14 concentration

Effect of initial AR14 concentration on the removal efficiency of AR14 was studied by varying the initial AR14 concentration (10, 20, 30, 60, 90, 120 mg/L) at constant adsorbent dosage (0.24 g/L) and at pH 3 (Fig. 8). When the initial AR14 concentration was increased from 10 to 120 mg/L, the AR14 removal efficiency was decreased from 99.99% to 30.86%. The reason for this result can be explained with the fact that the adsorbent has a limited number of active sites, which would become saturated above a certain AR14 concentration. Similar observations were also reported for the removal of dyes [34,35,38,43].

3.2.4. Effect of ionic strength

To assess the effect of different type of background electrolytes such as Cl^-, CO_3^{2-}, HCO_3^- and SO_4^{2-} on the removal efficiency of AR14, constant amounts of NaCl, Na_2CO_3, $NaHCO_3$ and Na_2SO_4 (30 mg/L) were added to the reactor

Fig. 9. The effect of ionic strength on the removal of AR14 dye by kaolin coated with Fe_3O_4 nanoparticles in different time interval (pH = 3, initial dye concentration = 30 mg/L, adsorbent dose = 0.24 g/L, 298 K).

before beginning the adsorption at constant concentration of AR14 (30 mg/L) and adsorbent dosage (0.24 g/L) at pH 3. Fig. 9 shows that removal efficiency of AR14 decreased in the presence of four selected anions. The order of removal efficiency was: control > sodium chloride > sodium carbonate > sodium bicarbonate > sodium sulfate. This removal trend can be explained by that Cl^-, CO_3^{2-}, HCO_3^- and SO_4^{2-} may interfere or compete the electrostatic attraction between SO_4^{2-} ions in AR14 species and surface of kaolin-Fe_3O_4 nanoparticles [43].

3.2.5. Comparison of each process, spectral changes and reusability

To evaluate effect of various processes on the removal efficiency of AR14, removal efficiency of AR14 by kaolin, magnetite, and kaolin-Fe$_3$O$_4$ nanoparticles were compared at the initial AR14 concentration (30 mg/L), adsorbent dosage (0.24 g/L) and at pH 3. Fig. 10 shows that removal efficiency for each process was 19.83%, 61.36% and 90.84%. These experiments demonstrate that both kaolin and Fe$_3$O$_4$ nanoparticles are needed for the effective removal of AR14. The changes in the absorption spectra of AR14 solutions at different time interval are shown in Fig. 11. The spectrum

Fig. 10. The contribution of each process involved on the AR14 dye by kaolin coated with Fe$_3$O$_4$ nanoparticles in different time interval (pH = 3, initial dye concentration = 30 mg/L, adsorbent dose = 0.24 g/L, 298 K).

Fig. 11. Spectral changes of AR14 dye solution by kaolin coated with Fe$_3$O$_4$ nanoparticles in different time interval (pH = 3, initial dye concentration = 30 mg/L, adsorbent dose = 0.24 g/L, 298 K).

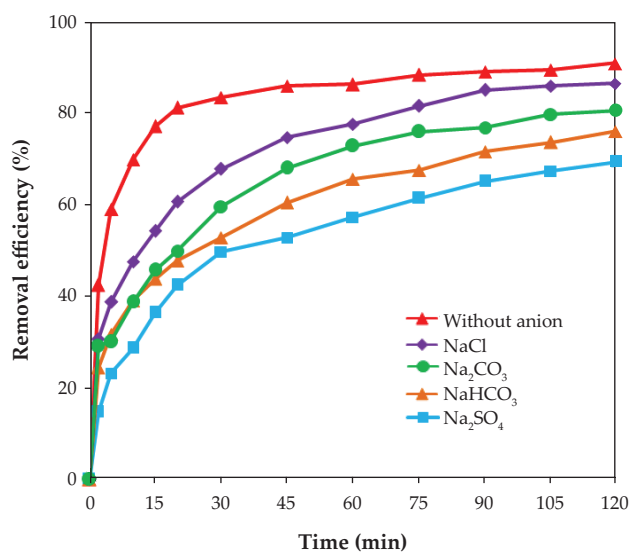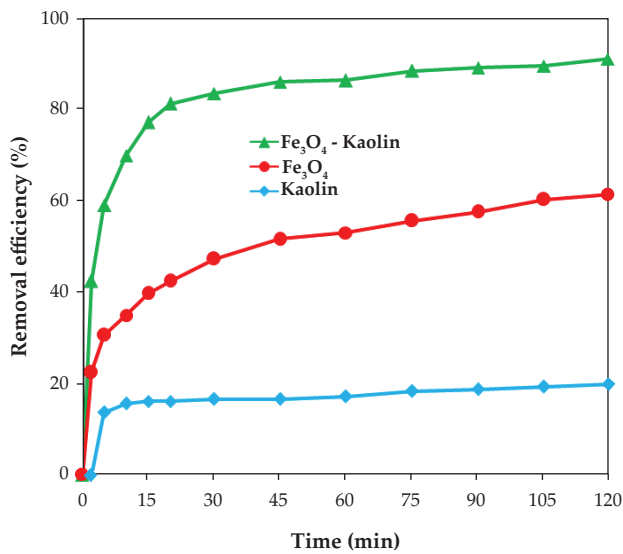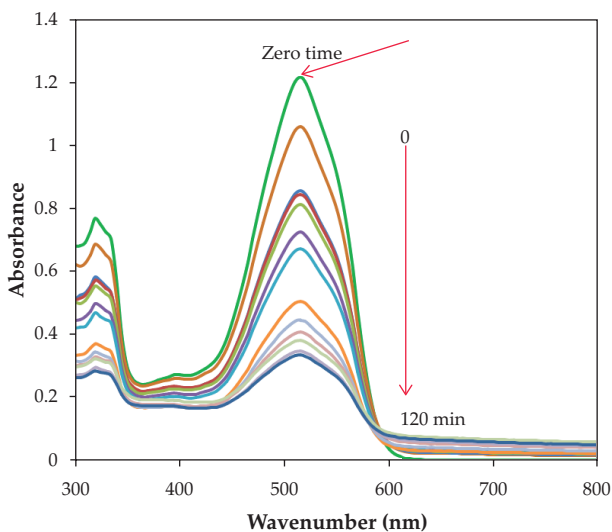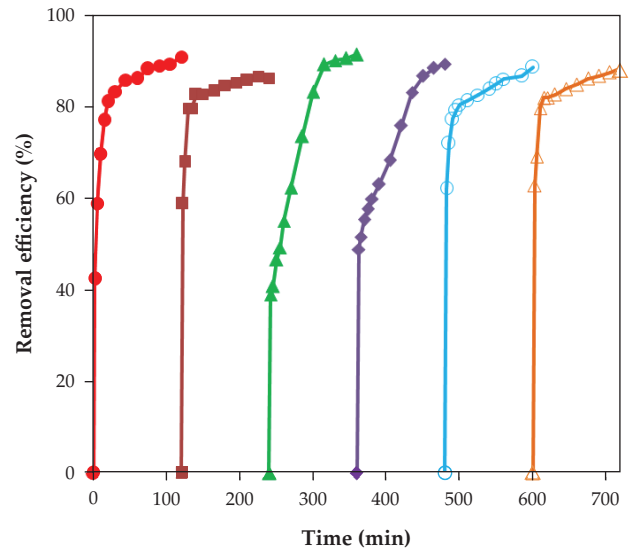Fig. 12. The results of reusability test for the removal of AR14 dye by kaolin coated with Fe$_3$O$_4$ nanoparticles in different time interval (pH = 3, initial dye concentration = 30 mg/L, adsorbent dose = 0.24 g/L, 298 K).

of AR14 in the visible region exhibits a main band with a maximum at 515 nm. The decrease of absorption peak of AR14 at 515 nm indicates rapid removal of the azo dye. Complete removal of AR14 was observed at 2 h in the optimized conditions. Reusability of adsorbent is an important factor for the application of developed adsorbent in the treatment of wastewater. Thus, NaOH solution (0.01 N) was used for the regeneration of the used adsorbent. A near complete desorption of AR14 from adsorbent by NaOH solution was occurred immediately. Hence, the cycle of adsorption and desorption of AR14 was repeated six times. It was observed that adsorption efficiency of AR14 by regenerated adsorbent was 90.84%, 86.18%, 91.4%, 89.31%, 88.59% and 88.43% at the end of the first, second, third, fourth, fifth, sixth cycle, respectively. The regenerated adsorbent can be applied to treat new wastewater containing AR14 until its removal capacity meets the emission standards for dyeing wastewater. As can be seen in Fig. 12, adsorption capacity of AR14 by kaolin-Fe$_3$O$_4$ nanoparticles was maintained up to six consecutive runs, suggesting a plausible adsorbent in the treatment of organic dyes.

3.3. Kinetic, equilibrium and thermodynamic studies

Adsorption kinetic experiments were performed at different AR14 concentration (10, 20, 30, 60, 90, 120 mg/L), at constant adsorbent dosage (0.24 g/L) and at pH 3. The pseudo-first-order, pseudo-second-order and intra-particle-diffusion model models were applied in order to find an efficient model for the description of adsorption. The relevant equations for the kinetic, equilibrium and thermodynamic studies are shown in Table 2 [47–49]. To obtain kinetic data for the removal of AR14, $\ln\left(1 - \dfrac{q_t}{q_e}\right)$ and $\dfrac{t}{q_2}$ versus t and

Table 2
The kinetic and isotherm and thermodynamic equations for adsorption of AR14 onto Kaolin-Fe$_3$O$_4$ nanoparticles

Kinetic models	Isotherm equations	Thermodynamic equations
Pseudo-first-order	Freundlich isotherm	Van't Hoff
$\ln\left(1-\dfrac{q_t}{q_e}\right)=-k_1 t$	$\log q_e=\log K_F+\dfrac{1}{n}\log C_e$	$\ln(K_l)=\dfrac{\Delta S}{R}-\dfrac{\Delta H}{RT}$
Pseudo-second-order	Langmuir isotherm	Free energy of adsorption
$\dfrac{t}{q_t}=\dfrac{1}{k_2 q_e^{\,2}}+\dfrac{1}{q_e}t$	$q_e=\dfrac{K_L q_m C_e}{1+K_L C_e}$	$\Delta G=-RT\ln K_L$
Intra-particle diffusion model	Separation factor (RL)	
$q_t=K_p\times t^{0.5}+C$	$R_L=\dfrac{1}{1+K_L C_0}$	

Parameters

q_e(mg/g), q_t(mg/g), k_1 (1/min), k_2 (g/mgmin), K_L (L/mg), q_m(mg/g), K_F(mg$^{1-1/n}$ L$^{1/n}$ g^{-1}, K_p (mg/g·min$^{-0.5}$), C_0 (mg/g), ΔS (J/mol.K), ΔH (kJ/mol), R (8.314 J/mol.K), T(K).

Table 3
The calculated kinetic parameters for pseudo-first-order, pseudo-second-order and intra-particle diffusion models for removal of AR14 dye by with Kaolin-Fe$_3$O$_4$ nanoparticles

Pseudo-first-order model						Pseudo-second-order model				Intra-particle diffusion model			
C_0 (mg/L)	q_e (exp) (mg/g)	k_1 (1/min)	q_e (cal) (mg/g)	R^2	P value	k_2 (g/mg-min)	q_e (cal) (mg/g)	R^2	P value	K_p (mg/g· min$^{-0.5}$)	C_0 (mg/g)	R^2	P value
10	41.66	0.1998	42	0.9886	0.002	0.02	42.19	0.9997	0.003	14.04	20.046	0.5558	0.001
20	81.96	0.0495	82	0.926	0.016	0.0046	83.43	0.9996	0.000	11.138	33.145	0.6821	0.001
30	113.55	0.0343	114	0.9004	0.001	0.0034	114.95	0.9995	0.05	7.11	47.939	0.6631	0.001
60	118.87	0.0348	119	0.7559	0.132	0.0022	117.64	0.9947	0.014	7.445	50.157	0.6688	0.000
90	142.82	0.0421	143	0.9061	0.396	0.001	147.05	0.9959	0.000	5.63	37.56	0.8339	0.001
120	154.31	0.0323	155	0.8498	0.979	0.0003	169.49	0.974	0.000	2.63	10.903	0.9534	0.108

q_t versus $t^{0.5}$ was plotted for the pseudo-first-order, pseudo-second-order and intra-particle-diffusion models, respectively. The kinetic parameters for the removal AR14 at different initial AR14 concentrations by pseudo-first-order, pseudo-second-order and intra-particle-diffusion models are summarized in Table 3. The kinetic data for AR14 adsorption showed the best fitting ($R^2 = 0.9999$) with the pseudo-second-order model. Moreover, when the initial AR14 concentration increased from 10 to 120 mg/L, the value of k_2 (g/mg-min) and R^2 for the pseudo-second-order model were decreased from 0.14 to 0.007 g/mg-min and 0.9999 to 0.9944, respectively. Also, q_e (mg/g) increased from 41.66 to 227.27 mg/g. This result indicated that adsorption data were well fitted with this model. In addition, the suitability of data deducted from the pseudo-second-order confirms that the rate-limiting step in adsorption of AR14 by kaolin-Fe$_3$O$_4$ nanoparticles might be coming from electrostatic attraction phenomenon. The value of C was measured as 50.157 mg/g, indicating that intra-particle diffusion is not the only controlling step for AR14 adsorption and the process is controlled by boundary layer diffusion in some

degree. Also the kinetic data were fitted with the linear regression statistics method. The estimated p values for AR14 have been summarized in Table 3. From these results, kinetic data for AR14 adsorption was fitted well with the pseudo-second-order model ($p < 0.05$) compared with the other kinetic models.

To investigate the adsorption equilibrium isotherm, experiments were performed with 30 mg/L AR14 as an initial concentration using various adsorbent dosages (0.1–0.4 g/L) at pH 3 for 72 h. All experiments were repeated three times and the average values were reported. Langmuir and Freundlich equations were applied to fit experimental adsorption data, and the related equations are shows in Table 2. R_L value (separation factor) represents a characteristic of the Langmuir isotherm. Generally, adsorption will be favorable when R_L value is between 0 and 1. While unfavorable adsorption will be expected above 1 of R_L value, R_L value 1 and 0 means linear and irreversible adsorptions, respectively. Fig. 13 shows that the linear plot of c_e/q_e versus c_e gives a straight line of slope $1/q_m$ and intercept $1/k_L q_m$. The values of q_m and k_L at different temperature are given in Table 4. The value of correlation

Table 4
The isotherm and thermodynamic constants for the adsorption of AR14 dye by Kaolin-Fe_3O_4 nanoparticles

Temperature (K)	Adsorbent	Dyes	Freundlich constants			q_m (mg/g)	Langmuir constants		Thermodynamic parameters			Reference
			K_F (mg$^{1-1/n}$ L$^{1/n}$ g^{-1})	n	R^2		K_L (L/mg)	R^2	ΔG (KJ mol^{-1})	ΔH (KJ mol^{-1})^a	ΔS (J mol^{-1}K^{-1})	
299	Kaolin	brilliant green	16.24	0.35	0.97	65.42	0.17	0.99	–4.19	–8.85	–17.56	[20]
298	Kaolin (Q38)	congo red	1.98	4.12	0.9018	5.44	0.5	0.9953	–11.054	–16.968	–19.722	[37]
298	Kaolin (K15GR)	congo red	1.86	3.41	0.8292	6.81	0.23	0.9944	–11.054	–11.849	–2.66	[37]
299	Kaolin	crystal violet	15.12	0.29	0.97	47.27	0.25	0.99	–4.13	–0.14	14.28	[18]
299	Kaolin	brilliant green	16.24	0.35	0.97	65.42	0.17	0.99	–4.19	–8.85	–17.56	[18]
298	Cellulose/ Fe_3O_4/activated carbon	congo red	30.10	4.18	0.960	66.09	0.85	0.996	–4.602	–52.4	–0.158	[38]
313	Cellulose/ Fe_3O_4/activated carbon	congo red	22.66	3.22	0.986	62.94	0.64	0.998	–3.478	–	–	[38]
328	Cellulose/ Fe_3O_4/activated carbon	congo red	15.89	2.50	0.96	60.50	0.4	0.992	–			[38]
323	Cellulose/ Fe_3O_4/activated carbon	congo red	–	–	–	–	–	–	–0.349			[38]
295	Kaolin	Crystal Violet	15.12	0.29	0.971	47.27	0.25	0.996	–	–	–	[32]
293	Kaolin	Crystal Violet	–	–	–	–	–	–	4.35	–139.25	14.28	[32]
298	Fe_3O_4/ZrO_2/ Chitosan	amaranth	10.658	2.309	0.98	99.6	0.034	0.970	–	–	–	[39]
298	Fe_3O_4/ZrO_2/ Chitosan	tartrazine	8.529	2.544	0.972	47.3	0.06	0.913	–	–	–	[39]
298	Fe_3O_4@ graphene	Methylen Blue	8.10	1.83	0.981	45.27	0.183	0.995	–	–	–	[40]
298	Fe_3O_4@ graphene	Cresol Red	8.53	2.25	0.981	33.66	0.27	0.993	–	–	–	[40]
298	Fe_3O_4	neutral red	10.616	2.173	0.994	105	0.0451	0.992	–	–	–	[4]
298	Graphene-Carbon-Fe_3O_4	methylene blue	31.74	3.66	0.92	73.26	0.58	0.96	–	-	–	[34]
298	Kaolin-Fe_3O_4	AR14	7.6	0.99	0.5221	94.34	0.905	0.9804	0.247	–45.66	–153.97	This study
308	Kaolin-Fe_3O_4	AR14	5.02	1.012	0.5476	53.47	0.513	0.9752	1.7			This study
323	Kaolin-Fe_3O_4	AR14	1.93	0.88	0.768	34.12	0.218	0.9459	4.09			This study

^{a}Results of plotting $\ln K_L$ vs $1/T$: slope = 5492.5, intercept = –18.52, R^2 = 0.9994.
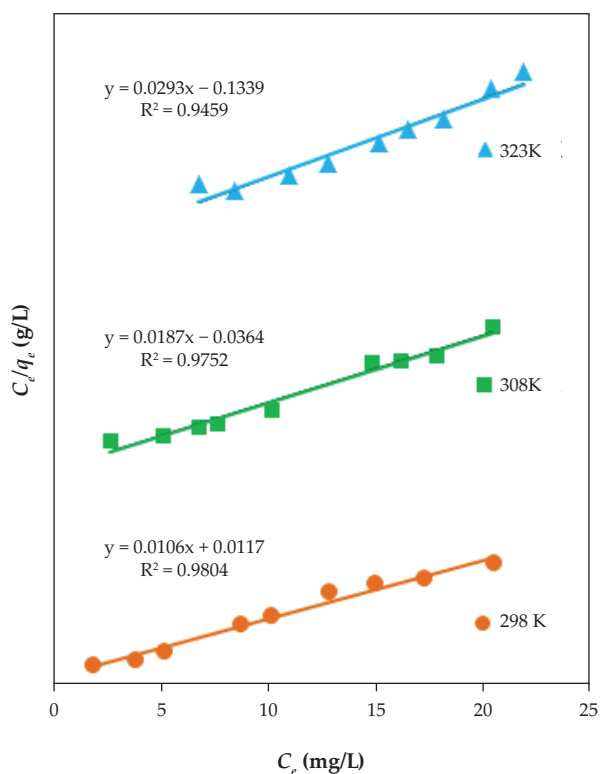
Fig. 13. Langmuir isotherm plots for the adsorption of the AR14 dye by kaolin coated with Fe_3O_4 nanoparticles at different temperatures.
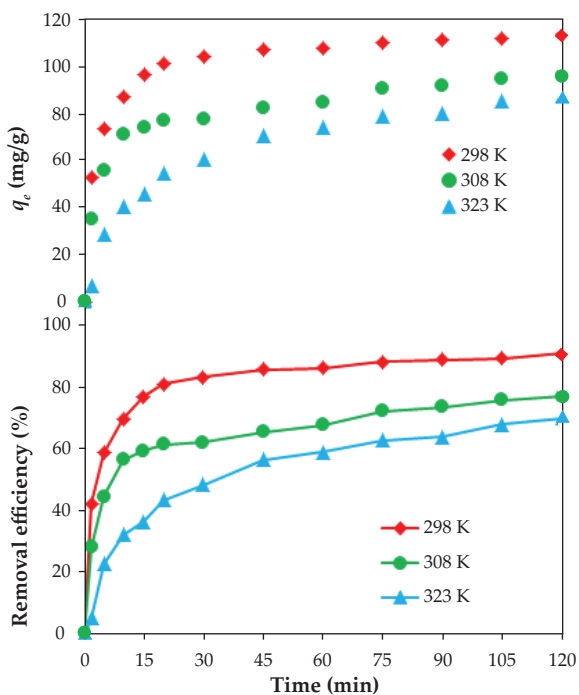

Fig. 14. The effect of temprature on the removal of AR14 dye by kaolin coated with Fe_3O_4 nanoparticles in different time interval (pH = 3, initial dye concentration = 30 mg/L, adsorbent dose = 0.24 g/L, 298 K).

coefficient $R^2 = 0.9804$, $R^2 = 0.9752$ and $R^2 = 0.9459$ at 298, 303, 323 K indicates that sorption of the AR14 onto the kaolin-Fe_3O_4 nanoparticles follows a Langmuir isotherm. The monolayer saturation capacity at temperature of 298, 303, and 323K is 94.34, 53.47 and 34.12 mg/g, respectively. It means that the adsorption of AR14 onto kaolin-Fe_3O_4 nanoparticles occurred as homogeneous and monolayer adsorption. Also, separation factor (R_L) at temperature of 298, 303, and 323 K was calculated as 0.05 to 0.368, 0.07 to 0.379 and 0.127 to 0.322, respectively. The applicability of the Freundlich sorption isotherm was also analyzed by plotting $\log(q_e)$ versus $\log(c_e)$, but data were not well fitted with Freundlich equation compared with the Langmuir equation. The Freundlich isotherm constants at different temperature are given in Table 4.

Thermodynamic experiments were performed at different temperature from 298 to 323 K at constant adsorbent dosage (0.24 g/L) and at pH 3 (Fig. 14). When the temperature was increased from 298 to 323 K, the AR14 removal efficiency was decreased from 90.84% to 70.14%. The related equations are shown in Table 2. From linear plot between $\ln K_L$ and $1/T$, ΔH (kJ mol^{-1}) and ΔS (J mol^{-1} K^{-1}) were calculated from the slope and intercept, respectively. The values of ΔS, ΔH, ΔG and q_m at different temperature are given in Table 4. Decreased removal efficiency at high temperature indicates an exothermic process (negative ΔH values) for the adsorption [8]. Similar result has been reported for removal of brilliant green [20] and crystal violet [32] by kaolin. The negative values of ΔS suggest a decrease in randomness and no significant changes in the internal structure of the adsorbents through the adsorption [8]. The removal capacity of AR14 by kaolin-Fe_3O_4 nanoparticles was compared with that by other adsorbents in Table 4. Kaolin-Fe_3O_4 nanoparticles have greater adsorption capacity than other adsorbents. Maximum adsorption capacity was obtained as 94.34 mg/g at pH 3. Based on the obtained results, the kaolin-Fe_3O_4 nanoparticles can be regarded as an efficient and low-cost adsorbent.

4. Conclusions

Super paramagnetic kaolin-Fe_3O_4 nanoparticles with average size 22 nm was used for the removal of AR14 dye from water. The prepared sample was characterized by FT-IR, XRD, SEM, EDX, and VSM. The removal efficiency depended on experimental parameters like the amount of adsorbent, contact time, pH and initial dye concentration. The removal efficiency was maximum at pH 3 and was increased with increasing contact time and adsorption dosage, but was decreased with increasing initial dye concentration and temperature. Pseudo-second-order model was better described the adsorption kinetics of AR14 onto adsorbent than pseudo-first-order model and intra-particle-diffusion models. The high value of correlation coefficient for the Langmuir isotherm suggests that adsorption occurs through homogeneous and monolayer adsorption. The maximum adsorption capacity of AR14 by kaolin-Fe_3O_4 nanoparticles was 94.34 mg/g at 298 K.

References

[1]   N. Daneshvar, M.H. Rasoulifard, A.R. Khataee, F. Hosseinzadeh, Removal of C.I. Acid Orange 7 from aqueous solution by UV irradiation in the presence of ZnO nanopowder, J. Hazard. Mater., 143 (2007) 95–101.

[2]   T. Robinson, G. McMullan, R. Marchant, P. Nigam, Remediation of dyes in textile effluent: a critical review on current treatment technologies with a proposed alternative, Bioresour. Technol., 77 (2001) 247–255.

[3]   R.J. Davis, J.L. Gainer, G. Neal, I.W. Wu, Photocatalytic decolorization of wastewater dyes, Water Environ. Res., 66 (1994) 50–53.

[4]   M. Iram, C. Guo, Y. Guan, A. Ishfaq, H. Liu, Adsorption and magnetic removal of neutral red dye from aqueous solution using Fe_3O_4 hollow nanospheres, J. Hazard. Mater., 181 (2010) 1039–1050.

[5]   A. Khataee., Removal of Azo Dye C.I.Acid Red 14 from Water using Fenton, UV/H_2O_2, $UV/H_2O_2/Fe(II)$, $UV/H_2O_2/Fe(III)$ and $UV/H_2O_2/Fe(III)/Oxalate$ Processes: A Comparative Study, J. Environ. Sci. Health, Pt. A: Toxic, Hazard. Subst. Environ. Eng., 41 (2006) 315–328.

[6]   N. Daneshvar, D. Salari, A.R. Khataee, Photocatalytic degradation of azo dye acid red 14 in water on ZnO as an alternative catalyst to TiO2, J. Photochem. Photobiol. A: Chem., 162 (2004) 317–322.

[7]   D. Ghosh, K.G. Bhattacharyya, Adsorption of methylene blue on kaolinite, Appl. Caly. Sci., 20 (2002) 295–300.

[8]   B.H. Hameed, A.A. Ahmad, N. Aziz, Isotherms, kinetics and thermodynamics of acid dye adsorption on activated palm ash, Chem. Eng. J., 133 (2007) 195–203.

[9]   M.S. Siboni, M. Samarghandi, J.-K. Yang, S.-M. Lee, Photocatalytic Removal of Reactive Black-5 Dye from Aqueous Solution by UV Irradiation in Aqueous TiO2: Equilibrium and Kinetics Study, J. Adv. Oxid. Technol., 14 (2011) 302–307.

[10] K. Soutsas, V. Karayannis, I. Poulios, A. Riga, K. Ntampegliotis, X. Spiliotis, G. Papapolymerou, Decolorization and degradation of reactive azo dyes via heterogeneous photocatalytic processes, Desalination., 250 (2010) 345–350.

[11] J. Wu, M. Eiteman, S. Law, Evaluation of Membrane Filtration and Ozonation Processes for Treatment of Reactive-Dye Wastewater, J. Environ. Eng., 124 (1998) 272–277.

[12] M.-X. Zhu, L. Lee, H.-H. Wang, Z. Wang, Removal of an anionic dye by adsorption/precipitation processes using alkaline white mud, J. Hazard. Mater., 149 (2007) 735–741.

[13] T. Pauporte, J. Rathouský, Electrodeposited mesoporous ZnO thin films as efficient photocatalysts for the degradation of dye pollutants, J. Phys. Chem. C., 111 (2007) 7639–7644.

[14] A. Alinsafi, M. Khemis, M. Pons, J. Leclerc, A. Yaacoubi, A. Benhammou, A. Nejmeddine, Electro-coagulation of reactive textile dyes and textile wastewater, Chem. Eng. Process., 44 (2005) 461–470.

[15] N. Daneshvar, D. Salari, A.R. Khataee, Photocatalytic degradation of azo dye acid red 14 in water: investigation of the effect of operational parameters, J. Photochem. Photobiol A: Chem., 157 (2003) 111–116.

[16] J.-S. Wu, C.-H. Liu, K.H. Chu, S.-Y. Suen, Removal of cationic dye methyl violet 2B from water by cation exchange membranes, J. Membr. Sci., 309 (2008) 239–245.

[17] A. Khataee, N. Daneshvar, M.H. Rasoulifard, F. Hosseinzadeh, Removal of C.I. Acid Orange 7 from aqueous solution by UV irradiation in the presence of ZnO, J. Hazard. Mater., 143 (2007) 95–101.

[18] B.K. Nandi, A. Goswami, M.K. Purkait, Removal of cationic dyes from aqueous solutions by kaolin: Kinetic and equilibrium studies, Appl. Caly. Sci., 42 (2009) 583–590.

[19] V.K. Gupta, A. Mittal, V. Gajbe, J. Mittal, Removal and Recovery of the Hazardous Azo Dye Acid Orange 7 through Adsorption over Waste Materials: Bottom Ash and De-Oiled Soya, Ind. Eng. Chem. Res., 45 (2006) 1446–1453.

[20] B.K. Nandi, A. Goswami, M.K. Purkait, Adsorption characteristics of brilliant green dye on kaolin, J. Hazard. Mater., 161 (2009) 387–395.

[21] V. Garg, R. Gupta, A.B. Yadav, R. Kumar, Dye removal from aqueous solution by adsorption on treated sawdust, Bioresour. Technol., 89 (2003) 121–124.

[22] T. Robinson, B. Chandran, P. Nigam, Removal of dyes from an artificial textile dye effluent by two agricultural waste residues, corncob and barley husk, Environ. Int., 28 (2002) 29–33.

[23] M. Shirzad-Siboni, S.J. Jafari, O. Giahi, I. Kim, S.-M. Lee, J.-K. Yang, Removal of acid blue 113 and reactive black 5 dye from aqueous solutions by activated red mud, J. Ind. Eng. Chem., 20 (2014) 1432–1437.

[24] S. Wang, Y. Boyjoo, A. Choueib, Z. Zhu, Removal of dyes from aqueous solution using fly ash and red mud, Water Res., 39 (2005) 129–138.

[25] G. Crini, Non-conventional low-cost adsorbents for dye removal: a review, Bioresour. Technol., 97 (2006) 1061–1085.

[26] Q.-Y. Zou, P. Yang, Y. Wang, L. Jia, Study on Adsorption of Congo Red in Water on Calcined Oyster Shell Powder [J], Technol. Develop. Chem. Ind., 6 (2010) 015.

[27] Z. Aksu, Biosorption of reactive dyes by dried activated sludge: equilibrium and kinetic modelling, Biochem. Eng. J., 7 (2001) 79–84.

[28] Y. Xue, H. Hou, S. Zhu, Adsorption removal of reactive dyes from aqueous solution by modified basic oxygen furnace slag: isotherm and kinetic study, Chem. Eng. J., 147 (2009) 272–279.

[29] G. Crini, P.-M. Badot, Application of chitosan, a natural aminopolysaccharide, for dye removal from aqueous solutions by adsorption processes using batch studies: A review of recent literature, Prog. Polym. Sci., 33 (2008) 399–447.

[30] M. Shirzad-Siboni, A. Khataee, S.W. Joo, Kinetics and equilibrium studies of removal of an azo dye from aqueous solution by adsorption onto scallop, J. Ind. Eng. Chem., 20 (2014) 610–615.

[31] K.A. Tan, N. Morad, T.T. Teng, I. Norli, P. Panneerselvam, Removal of Cationic Dye by Magnetic Nanoparticle (Fe_3O_4) Impregnated onto Activated Maize Cob Powder and Kinetic Study of Dye Waste Adsorption, APCBEE Procedia., 1 (2012) 83–89.

[32] B.K. Nandi, A. Goswami, A.K. Das, B. Mondal, M.K. Purkait, Kinetic and Equilibrium Studies on the Adsorption of Crystal Violet Dye using Kaolin as an Adsorbent, Sep. Sci. Technol., 43 (2008) 1382–1403.

[33] A.R. Tehrani-Bagha, H. Nikkar, N.M. Mahmoodi, M. Markazi, F.M. Menger, The sorption of cationic dyes onto kaolin: Kinetic, isotherm and thermodynamic studies, Desalination., 266 (2011) 274–280.

[34] W. Fan, W. Gao, C. Zhang, W.W. Tjiu, J. Pan, T. Liu, Hybridization of graphene sheets and carbon-coated Fe_3O_4 nanoparticles as a synergistic adsorbent of organic dyes, JMCh., 22 (2012) 25108–25115.

[35] N. Yang, S. Zhu, D. Zhang, S. Xu, Synthesis and properties of magnetic Fe_3O_4-activated carbon nanocomposite particles for dye removal, Mater. Lett., 62 (2008) 645–647.

[36] Z. Zhang, J. Kong, Novel magnetic Fe_3O_4@C nanoparticles as adsorbents for removal of organic dyes from aqueous solution, J. Hazard. Mater., 193 (2011) 325–329.

[37] V. Vimonses, S. Lei, B. Jin, C.W.K. Chow, C. Saint, Adsorption of congo red by three Australian kaolins, Appl. Caly. Sci., 43 (2009) 465–472.

[38] H.Y. Zhu, Y.Q. Fu, R. Jiang, J.H. Jiang, L. Xiao, G.M. Zeng, S.L. Zhao, Y. Wang, Adsorption removal of congo red onto magnetic cellulose/Fe_3O_4/activated carbon composite: Equilibrium, kinetic and thermodynamic studies, Chem. Eng. J., 173 (2011) 494–502.

[39] H. Jiang, P. Chen, S. Luo, X. Luo, X. Tu, Q. Cao, Y. Zhou, W. Zhang, Synthesis of Novel Biocompatible Composite Fe_3O_4/ZrO_2/Chitosan and Its Application for Dye Removal, J. Inorg. Organomet. Polym., 23 (2013) 393–400.

[40] Y. Yao, S. Miao, S. Liu, L.P. Ma, H. Sun, S. Wang, Synthesis, characterization, and adsorption properties of magnetic Fe_3O_4@graphene nanocomposite, Chem. Eng. J., 184 (2012) 326–332.

[41] B. Qu, J. Zhou, X. Xiang, C. Zheng, H. Zhao, X. Zhou, Adsorption behavior of azo dye C. I. acid red 14 in aqueous solution on surface soils, J. Environ. Sci. (China), 20 (2008) 704–709.

[42] S. Nethaji, A. Sivasamy, A. Mandal, Preparation and characterization of corn cob activated carbon coated with nano-sized magnetite particles for the removal of Cr (VI), Bioresour. Technol., 134 (2013) 94–100.

[43] M. Farrokhi, S.-C. Hosseini, J.-K. Yang, M. Shirzad-Siboni, Application of ZnO–Fe$_3$O$_4$ Nanocomposite on the Removal of Azo Dye from Aqueous Solutions: Kinetics and Equilibrium Studies, Water. Air. Soil. Pollut., 225 (2014) 1–12.

[44] W.E. Federation, A.P.H. Association, *Standard methods for the examination of water and wastewater, American Public Health Association (APHA)*, Washington, DC: USA. (2005)

[45] M. Shirzad-Siboni, M. Farrokhi, R. Darvishi Cheshmeh Soltani, A. Khataee, S. Tajassosi, Photocatalytic reduction of hexavalent chromium over ZnO nanorods immobilized on kaolin, Ind. Eng. Chem. Res., 53 (2014) 1079–1087.

[46] A. Akbari, M. Homayonfal, V. Jabbari, Effect of solution chemistry and operating conditions on the nanofiltration of acid dyes by a nanocomposite membrane, Water Sci. Technol., 64 (2011) 2655–2663.

[47] Y. Liu, Y.-J. Liu, Biosorption isotherms, kinetics and thermodynamics, Sep. Purif. Technol., 61 (2008) 229–242.

[48] M. Shirzad-Siboni, M. Samarghandi, S. Azizian, W. Kim, S. Lee, The removal of hexavalent chromium from aqueous solutions using modified holly sawdust: equilibrium and kinetics studies, Environ. Eng. Res., 16 (2011) 55–60.

[49] M. Samarghandi, S. Azizian, M.S. Siboni, S. Jafari, S. Rahimi, Removal of divalent nickel from aqueous solutions by adsorption onto modified holly sawdust: equilibrium and kinetics, Iran. J. Environ. Health. Sci. Eng., 8 (2011) 167–174.